Evolution of epitaxial graphene layers on 3C SiC/Si (111) as a function of annealing temperature in UHV

B.Gupta[1], M.Notarianni[1], N.Mishra[2], M.Shafiei[1], F.Iacopi[2], N.Motta[1*]

[1] *Institute for Future Environments and School of Chemistry, Physics and Mechanical Engineering, Queensland University of Technology, 2 George Street, Brisbane 4001, QLD, Australia*

[2]*Queensland Micro and Nanotechnology Centre, Griffith University, Nathan Campus 4111, QLD Australia*

ABSTRACT

The growth of graphene on SiC/Si substrates is an appealing alternative to the growth on bulk SiC for cost reduction and to better integrate the material with Si based electronic devices. In this paper, we present a thorough in-situ study of the growth of epitaxial graphene on 3C SiC (111)/Si (111) substrates via high temperature annealing (ranging from 1125˚C to 1375˚C) in ultra high vacuum (UHV). The quality and number of graphene layers have been investigated by using X-ray Photoelectron Spectroscopy (XPS), while the surface characterization have been studied by Scanning Tunnelling Microscopy (STM). Ex-situ Raman spectroscopy measurements confirm our findings, which demonstrate the exponential dependence of the number of graphene layer from the annealing temperature.

* Corresponding Author: N. Motta (n.motta@qut.edu.au)

1. INTRODUCTION

Graphene attracts enormous interest due to its outstanding electrical [1], optical [2], thermal [3] and mechanical [4] properties. Its novel properties also include an anomalous Quantum Hall Effect (QHE) [5], the Klein tunnelling phenomenon [6] and weak (anti) localisation effects. Moreover, the high mobility and near ballistic transport at room temperature makes it a potential material for nanoelectronics and high frequency applications [7-11]. Due to its extraordinary properties[12], graphene could be used to overcome silicon device limitations, especially regarding the high charge mobility [13, 14]. Monolayers and bilayers of graphene are zero-gap semiconductors with one type of hole and one type of electron while for three or more layers several charge carriers appear. The limit between graphene and graphite has been set at 10 layers by some authors [7][15].

Several techniques have been developed and used to produce graphene in large quantities. The most common techniques include micromechanical exfoliation of highly oriented pyrolytic graphite (HOPG) [5], chemical vapour deposition (CVD) [7, 16] chemical reduction of graphite oxide (GO) [17], carbon nanotubes (CNTs) unzipping [18, 19], and epitaxial growth on bulk silicon carbide (SiC) [20, 21]. The successful development of graphene based nanoelectronics and sensors depends upon the availability of high quality and large area graphene layers directly grown on the device location on a wafer. In this regard, the above-mentioned methods each have their own limitations. The micromechanical cleavage offers no control over the number of layers and is not suitable for large scale production. The CVD method can produce large area graphene, but it requires a purification process to eliminate the catalyst particles and transfer of graphene to another substrate. Chemical reduction of GO and or CNT unzipping requires chemicals, which can affect

graphene properties. Preparation of graphene layers by thermal decomposition of SiC has been proposed as a promising method for the synthesis of homogeneous, wafer-size graphene layers for technological applications [22]. The formation of graphite by annealing of SiC surfaces in UHV was studied many years before the discovery of graphene [23, 24]. Van Bommel et al. [25] investigated the graphitization of SiC(0001) in 1975 for the first time. However, commercial SiC substrates remain limited in size and are very expensive. This could be a major limitation for the development of graphene based devices, such for example micro- and nano gas sensors[26], high frequency or logic transistors [27].

To address this issue, heteroepitaxial growth of cubic polytype (3C) SiC on silicon substrates has been proposed[28]. The high quality growth of 3C SiC/Si is challenging in terms of film uniformity and defects density arising from lattice and thermal mismatch of Si and SiC[29]. Large efforts have been made to improve these aspects and achieve a smooth and uniform 3C SiC/Si surface over large areas [29, 30]. The advantages of growing 3C SiC (111) on Si are threefold. First of all the Si substrate is cheaper and available in substantially larger areas than the commercial SiC wafers, and fully compatible with the current Si processing techniques, making graphene technology more attractive from an industrial point of view. Second, the graphitization of 3C SiC epilayers has been shown to produce ultra-thin carbon sheets like monolayer, bilayer or multilayer graphene [23, 31] on SiC/Si without the difficulty of transferring the material to an insulating substrate [32-34]. Third, the graphitization on the surface of 3C SiC (111) proceeds in a similar manner to that on the Si-terminated hexagonal bulk SiC crystals. This is because their crystallographic structure is quite similar [35] as this crystal also naturally accommodate the six-fold symmetry [36].

In this study we report the growth of graphene on 3C SiC (111)/Si (111) substrates at different temperatures ranging from 1125℃ to 1375℃. The growth, composition and structure of the graphene layers have been investigated in detail using X-ray photoelectron

spectroscopy (XPS), scanning tunnelling microscopy (STM) and Raman spectroscopy. All the experiments, except the Raman spectroscopy, have been performed in-situ, starting from the annealing of the SiC/Si (111) sample, followed by the STM and the XPS.

2. EXPERIMENTAL

A 250 nm thin film of 3C SiC (111) was grown at 1000 ˚C on on-axis 150 mm p-doped Si (111) wafer by alternating supply epitaxy (ASE) [30]. This process was undertaken in a hot-wall low-pressure CVD reactor using alternate supply of the vapour precursors silane (SiH_4) and cyclopropane (C_3H_6). Temperature was lowered to 950˚C during exposure to the carbon gas. Film thickness was monitored by Raman spectroscopy, while residual stress was measured from wafer curvature. The quality of the film and the epitaxial relationship with the substrate has been measured by X-Ray Diffraction and Transmission Electron Microscopy. See Ref [29] for further details. The roughness of the grown SiC was found to be 2.5 nm by analysing AFM and STM 5x5 μm images. The 3C SiC/Si (111) sample was cleaned stepwise in isopropyl alcohol and deionised water under sonication for 5 minutes and 2 minutes, respectively. After insertion in the UHV chamber the substrate was firstly degassed at 600 °C for 12 hrs in UHV and then annealed under a constant Si flux (0.11 nm/min) at 950 °C for 10 mins ($p_{max}=3\cdot10^{-10}$) in order to remove the native oxide from the surface and to compensate for the Si sublimation in the final step. Silicon was deposited by an e-beam evaporator (EFM 3, Omicron Nanotechnology) operated at 500V, 40mA. The source material was a silicon bar (Siliciumbearbeitung Andrea Holm GmbH, purity > 99.9999%) n-doped with phosphorous (10-100 Ω·cm). While this process removes the oxygen contamination in the form of silicon oxide (SiO), a volatile reaction product, it also prevents the formation of a thick graphite layer in the following step by reacting with non-carbidic form of C to form SiC [37, 38]. Afterward, epitaxial graphene layers were obtained by Si sublimation, using direct current

heating in UHV starting from a base pressure of $1 \cdot 10^{-10}$ mbar. This final annealing step ($p_{max}=5 \cdot 10^{-10}$) was carried out for 10 mins at temperatures ranging from 1125 to 1375˚C. The uncertainty on the sample temperature, measured by infrared optical pyrometer, was ±15 °C. The schematic diagram in Figure 1 shows the growth procedure.

The morphology and the electrical characteristics of the epitaxial graphene grown on the 3C SiC/Si (111) substrate were investigated in-situ just after the growth by STM (VT STM XA, Omicron Nanotechnology), by keeping the pressure at 2×10^{-11} mbar. After that, the chemical composition of the samples was characterized in the same UHV system by XPS using a non-monochromatic Mg Kα (1253.6 eV) X-ray source (DAR 400, Omicron Nanotechnology), 300W incident angle at 65° to the sample surface, with a 125 mm hemispherical electron energy analyser (Sphera II, 7 channels detector, Omicron Nanotechnology). Photoelectron data were collected at a take-off angle of 90°. Survey scans were taken at analyser pass energy of 50 eV and high resolution scans at 20 eV. The survey scans were carried out with 0.5 eV steps and a dwell time of 0.2 s, whereas high-resolution scans were run with 0.2 eV steps and 0.2 s dwell time. The pressure in the analysis chamber during XPS scans was kept below 4.0×10^{-10} mbar. The quality of the epitaxial graphene was also analysed ex-situ by Raman spectroscopy at room temperature using an "inVia Renishaw Raman microscope" with λ=532 nm. A 50% laser power (35 mW, spot size ~ 1 micron) was used with a 'X50' objective.

3. RESULTS AND DISCUSSION

Scanning Tunnelling Microscopy

Atomic structure of the epitaxially grown graphene on 3C SiC (111)/Si(111) was investigated by Scanning Tunneling Microscopy in Ultra High Vacuum. Figure 2 shows the STM

topographical image of monolayer graphene obtained at room temperature after annealing SiC at 1250 ˚C. The hexagonal structure of monolayer graphene (1×1) is clearly visible with periodicity (hole to hole) of 0.246 nm.

The graphene layer appears to be continuous on the substrate, although wrinkled because of the steps and defects in the underlying SiC/Si(111). STM images of graphene layers obtained after annealing at 1300 ˚C are shown in Fig. 3. Figure 3a is a 20x20 nm STM image showing a step where a Moiré pattern is visible like a shadow around the center of the image, while in two areas (top and bottom part of the image) it is even possible to observe the honeycomb graphene structure. This difference is due to the presence of multiple/single graphene layers in different areas of the sample and to the bias paramenters used (V_{bias} 70 mV, I=0.3nA).

The Moiré pattern, which is due to an electronic effect of interference between the first and second graphene layer [39] is more clear at a lower sample bias (V_{bias} 50 mV, I=0.2nA) (Figure 3b) showing a periodicity of 17Å. This structure is attributed to the C-rich (6√3×6√3) R30˚ reconstruction because of the 30˚rotation of the graphene overlayer with respect to the unreconstructed 3C SiC (111) surface [21, 40, 41]. In our case the typical structure due to the Bernal stacking is visible, confirming the presence of more than one graphene layer.

The unit cell of (6√3×6√3) R30˚ structure, shown in Figure 3b (blue insert), consists of (13×13) graphene unit cells[41]. The FFT of the Figure 3b is shown in Figure 3c. In this image, three sets of bright spots are visible, corresponding to the first and second nearest neighbours and to the Moirè pattern. From the angle measurements (Figure 3c), we observed that the graphene layer was rotated 27˚ ± 3˚ with respect to the buffer layer. A high resolution image of bilayer graphene is presented in Figure 3d, where the typical Bernal stacking symmetry with a periodicity of 0.246 nm is visible on the Moiré pattern. The STM image of

multilayer graphene at atomic scale exhibit the typical three-for-six symmetry of graphite. In order to disentangle all the contribution to the STM image, we have performed the back Fourier transform by selecting the different hexagons of bright spots in fig 3c (Fig 4).

The innermost, middle and outermost hexagons in Figure 3c are the Fourier components of the Moiré structure, second nearest and first nearest neighbour of graphene atoms, respectively. The periodicity of these structures as measured in 4a-c gives a value of the spacing equal to 17 Å, 4.2 Å and 2.46 Å, respectively, which confirm the quality of our graphene. Although the graphene domains are small, it is possible to increase their size up to several μm^2 by using off axis substrates as recently suggested by Ouerghi et al [42].

X-ray Photoelectron Spectroscopy

A full XPS analysis of the samples was performed after each step of the growth process, immediately following the STM measurements. Figure 5 shows the wide range XPS spectra of the sample after degassing at 600˚C, annealing with Si flux at 950˚C and final annealing at 1375˚C, respectively. The degassed sample spectrum shows the presence of six main photoelectron peaks at approximately 1000, 750, 570, 283, 150 and 100 eV which originate from the C KLL, O KVV, O1s, C1s, Si2s and Si2p transitions, respectively. The peaks related to oxygen (O KVV and O 1s) are reduced after annealing at 950˚C with Si flux and disappear after the annealing at 1375˚C (Figure 5).

After annealing at 950˚C under Si flux, the formation of a Si-rich (3×3) surface is observed [37, 43]. A comparison between the high-resolution XPS spectra obtained at 650˚C and 950˚C for both C1s (283.1eV) and Si2p (100.9 eV) peaks is shown in Figure 6. After 950˚C annealing we observe an slight increase (0.75 vs 0.68) in the intensity ratio of the Si2p peak with respect to the C1s, and the disappearing of the two side peaks in the Si2p confirming the effect of the Si evaporation in removing the SiO_2 and in increasing the Si/C ratio at the

surface. A very small shoulder at about 285 eV can be noticed in the C1s spectrum after annealing at 950 ˚C. The energy of this line obtained from the XPS fitting (285.04 eV) is very close to the peak of the buffer layer found in successive annealing treatment, indicating the onset of the formation of buffer layer [21].

Figure 7 (a-f) shows the evolution of the C1s peak at successive annealing temperatures (1125, 1225, 1250, 1275, 1325 and 1375˚C). Three peaks were used to fit the original spectra of C1s, corresponding to SiC (~ 283 eV), graphene (G=284.7 eV) and buffer layer (I = 285.85 eV). The transition of a Si-rich to C-rich surface is obtained by the sublimation of Si atoms taking place at annealing temperatures larger than 1125°C and resulting in the formation of a (6√3×6√3) R 30˚structure [21, 44]. At 1125°C (Figure 7a), a new component at 285.85 eV, identified as the buffer layer peak, begins to develop aside the main SiC bulk peak at 283.0eV. This is attributed to the transition of Si-rich surface to C-rich surface [40]. The buffer layer is usually the first carbon layer partially covalently bound to the SiC substrate and has no graphitic carbon sp^2 properties [21]. This layer has a typical (6√3×6√3) R 30˚ reconstruction as seen in the STM images [40, 44, 45]. The third peak at 284.7eV is assigned to graphene, as it is only 0.3eV behind the typical graphitic carbon peak. Around 1225°C (Figure 7b), higher intensities for both surface components, I and G are observed. The intensities and atomic concentrations (%) of G and carbon peak of SiC are listed in Table 1.

The number of graphene layers *t* formed on SiC can be calculated from the intensity ratio of the photoelectrons of graphene (N_G) and SiC as a reference peak (N_R) [46]:

$$\frac{N_G}{N_R} = \frac{T(E_G)\rho' C_G \lambda'(E_G)\left[1-\exp(-t/\lambda'(E_G))\right]}{T(E_R)\rho C_R \lambda(E_R)\exp(-t/\lambda(E_R))} \cdot F \qquad (1)$$

Where E is the kinetic energy of photoelectrons associated with a given peak, T is the transmission function of the analyser; C is the differential cross section ($d\sigma/d\Omega$). ρ and λ are the atomic density and inelastic mean free path of the corresponding material. F is a geometrical correction factor due to photoelectron diffraction and the superscript $'$ indicates quantities referred to the graphene over layer as opposed to the SiC bulk. The inelastic mean free path λ of SiC and of graphite was taken from the TPP-2M formula [47]. By solving the equation (1) for the number of layers t, and considering an interlayer spacing of 3.35 Å for the graphene, we can calculate the number of layers at the various annealing temperatures (Table 2).

At 1125 the number of layers is 0.4, as expected as we are below the onset of graphene growth. The calculated thickness value at 1225˚C (1.78) confirms already the presence of more than one monolayer graphene. At 1250°C (Figure 7c) the calculated thickness is 3 ML. The increase of the graphene peak intensity and decrease of SiC peak intensity (Figure 7c-f) indicates the formation of an increasing number of graphene layers as a function of the annealing temperature, while no change was observed for the buffer layer peak intensity as expected. A saturation of the graphene layer peak corresponding to a thickness of 7.8 ML was observed for annealing temperatures above 1325°C, which is most probably due to the limitation in the escape depth of the photoelectrons (about 1 nm at 1000 eV[48]). We note that 1375°C is also very close to the maximum safe annealing temperature of 3C SiC (111)/Si(111), as the melting point of silicon is 1414°C .

Raman spectroscopy

Raman characterization was performed ex-situ at room temperature immediately after extracting the samples annealed at different temperatures from the UHV. Figure 8 show the

Raman spectra of samples annealed at 1125˚C, 1225˚C, 1300˚C, 1325˚C and 1375˚C, including bulk graphite as a reference spectrum and the untreated 3C SiC/Si (111) substrate. In the graphite spectrum, the two most intense features, G and 2D peak, are visible at wavelengths 1580.46 and 2720.06 cm^{-1}, respectively. The G band is associated with doubly degenerate in-plane transverse optic (iTO) and longitudinal optic (LO) phonon mode at the Brillouin zone centre. It is the only band coming from a normal first order Raman scattering process in the graphene. The D and 2D (G') bands originates from a second order process, involving two iTO phonons near the K point for the 2D band or one iTO phonon and one defect in the case of the D-band [49]. The change in intensity and shift in position of both G and 2D peak is the key to determine the graphene layer thickness [49, 50].

From Table 3, the G-band position shifts towards lower wavelengths as the temperature increases, indicating the increase in graphene layer thickness; this is confirmed by the shift of the 2D band to higher wavelengths [50]. The lack of 2D peak for the sample annealed at 1125˚C is a signature that no or very little graphene is formed at this temperature. The peak position and FWHM for a CVD monolayer graphene (with 532 nm laser wavelength) have been reported as ~2680 cm^{-1} and ~28cm^{-1}, respectively [51], while for the micromechanically cleaved graphene is 2673 cm^{-1} [52].

At 1225˚C the 2D position of the Raman peak (2712 cm^{-1}) is very close to values reported in the literature for monolayer graphene on SiC (2715 cm^{-1}) [52], in good agreement with our XPS results, with a 39cm^{-1} shift towards higher frequency in comparison with the micromechanically cleaved graphene. This shift is not surprising, as it was also observed by other researchers [40, 52] in SiC graphitization, and attributed to the interaction of graphene with the SiC substrate, where strain changes the lattice constant of graphene and hence the Raman peak frequency [40]. The peak broadening can be attributed to the poor crystallinity and to the small size of the platelets of the epitaxial graphene [52] as suggested by our STM

images. A calculation of the crystallite size (L_a) from the intensity of G and D peaks I_G and I_D by using the formula [53] $L_a(\mathrm{nm}) = (2.4\times10^{-10})\lambda^4\left(\frac{I_G}{I_D}\right)$ (λ= 532 nm in this work) gives an average dimension of the graphene platelets of 10 -15 nm depending on the annealing temperature. By increasing the annealing temperature the width of both G and 2D peaks is decreasing, suggesting an improvement of the crystalline quality and an enlargement of the graphene areas. At 1375˚C, the G and 2D peaks are very close to the bulk graphite position indicating that at this temperature we have obtained thick graphene layers, confirming our XPS results. The presence of D-band (1363 cm^{-1}) (Figure 8) is a signature of defects caused by structural disorder, vacancies, distortions and strain [52, 54]. The other feature observed at around 2965 cm^{-1} is attributed to the combination of the D and G bands, known as D+G band [55]. Our 3C SiC/Si(111) substrate do not show any sign of significant second order Raman features between 1450 and 1750 cm^{-1} [49, 52] as in other polytypes of SiC.

Evaluation of the growth rate

In order to understand the growth rate as a function of the temperature we plotted the layer thickness developed after 10' annealing, obtained by the XPS analysis, as a function of the annealing temperature (Fig 9), and fitted the data by using the Arrhenius formula:

$$N(T) = A\, e^{-E_a/KT} \qquad (2)$$

We obtained A=1.81 10^7, and E_a=1.67 eV (activation energy). Interestingly the Raman 2D peak intensity follows the same behaviour (blue squares), as well as the G peak intensity (not shown in the graph). We excluded the XPS value obtained at 1375 ˚C from the fitting because of the error due to the limitation in the photoelectron escape depth as discussed in the XPS analysis.

4. CONCLUSIONS

We demonstrated that the number of graphene layers obtained by sublimation in UHV from 3C SiC (111)/Si(111) is a strong function of the annealing temperature. By quantitative XPS and Raman analysis we have been able to calculate the exact number of layers of epitaxially grown graphene. From the experimental results we infer that monolayer graphene can be grown in 10' by annealing 3C SiC(111)/Si(111) substrates at temperatures as low as 1200˚C. The STM analysis provided atomic scale images demonstrating the presence of mono or few layer graphene, depending on the annealing temperature; although a high number of defects is clearly visible, as confirmed by the presence of a D band in the Raman spectroscopy. We also observed on improvement of the graphene quality for increasing annealing temperatures, but also an increase in the number of layers. The final number of graphene layers increases up to about 8 ML for temperatures as high as 1375 ˚C, just below the melting temperature of the silicon substrate. We have been able to fit this behaviour to an Arrhenius function, which provides the onset temperature for the first layer and the activation energy of the SiC decomposition process into graphene. This study opens the way to a better understanding and quantification of the graphene growth in UHV from 3C SiC(111)/Si(111), which can be of utmost importance in future electronic applications. Further studies are in progress.

5. ACKNOWLEDGEMENTS

The authors acknowledge the support of the Australian Research Council (ARC) through the Discovery project DP130102120, the Marie Curie International Research Staff Exchange Scheme Fellowship within the 7th European Community Framework Programme, and the

Australian National Fabrication Facility. FI is recipient of a Future Fellowship from the Australian Research Council (FT120100445). The technical help of Mr. Robert Russell for Matlab calculations is kindly acknowledged. The technical support of Dr. P. Hines and Mr. W. Kwiecien of the Institute for Future Environments at QUT and the equipment of the Central Analytical Research Facility (CARF), as well as the funding by the ARC through the LIEF grant (LE100100146) are also kindly acknowledged. This work was performed in part at the Queensland node of the Australian National Fabrication Facility (ANFF) - a company established under the National Collaborative Research Infrastructure Strategy to provide nano and microfabrication facilities for Australia's researchers.

FIGURES

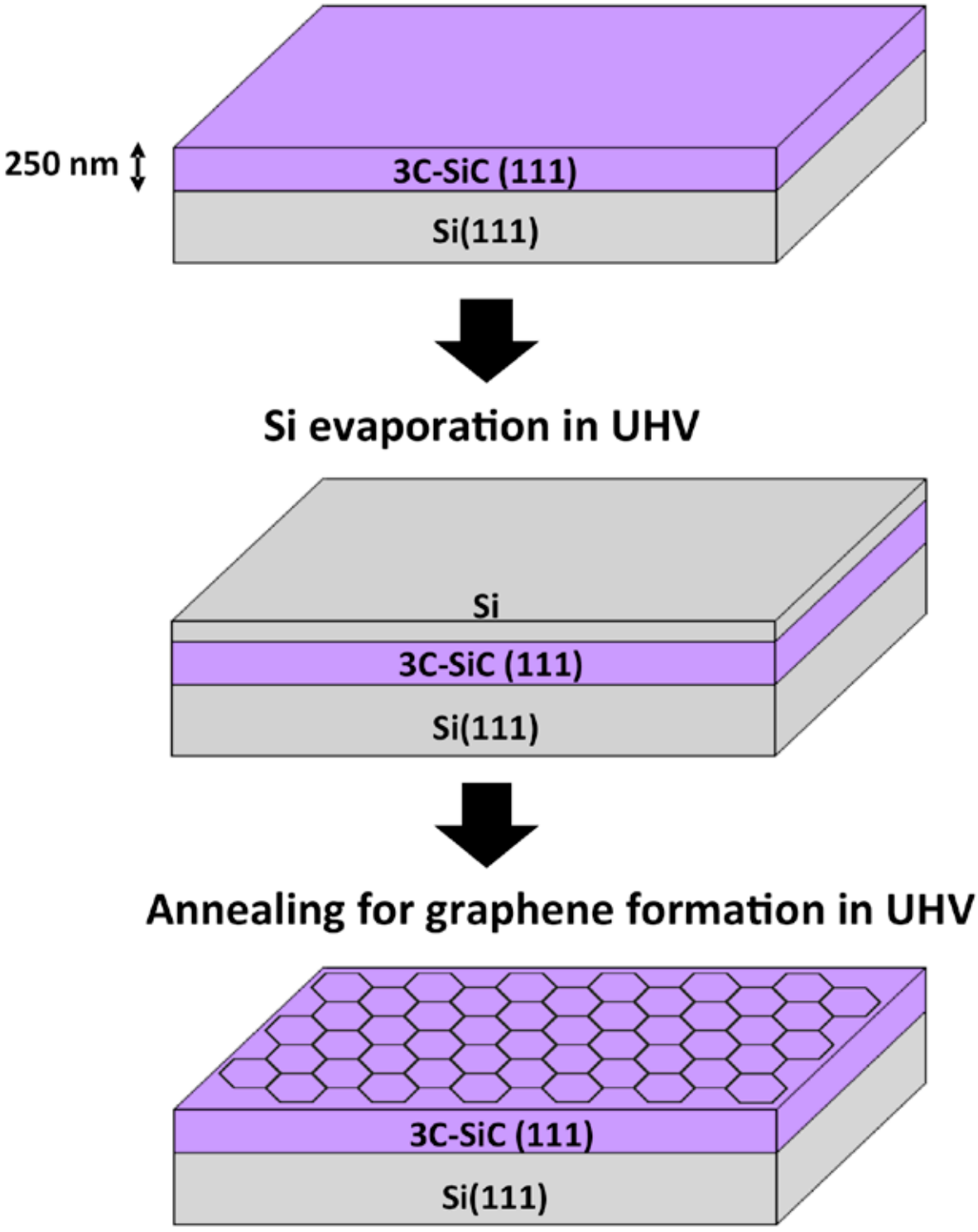

Figure 1 - Schematic diagram of graphene epitaxial growth process.

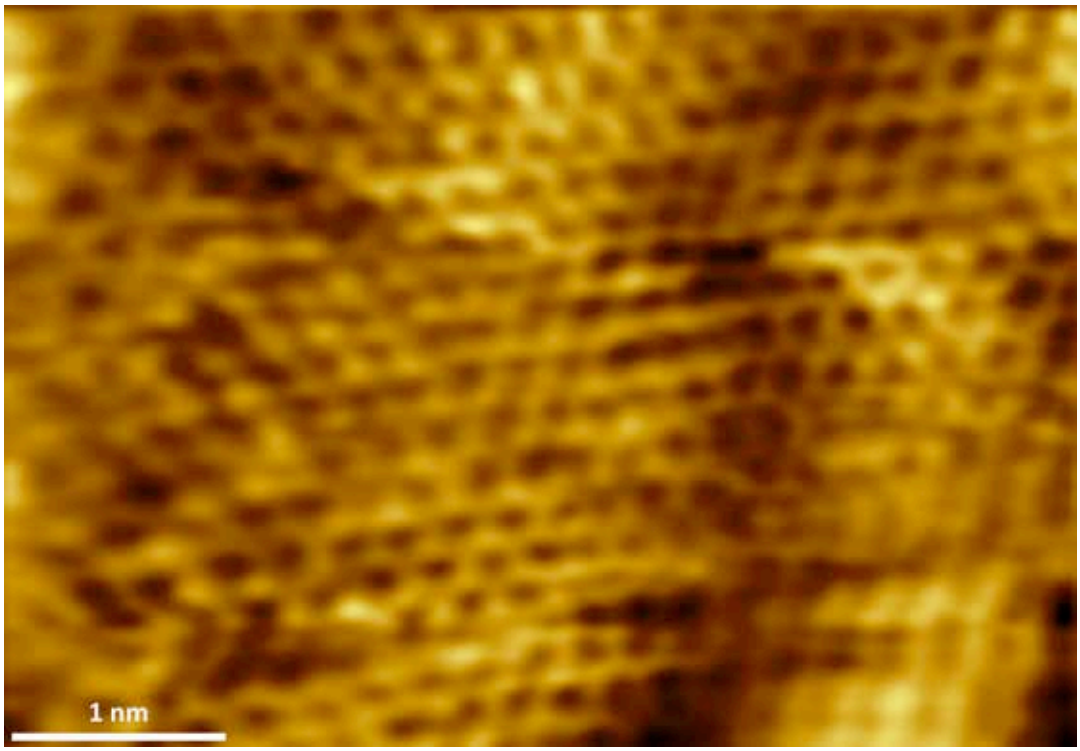

Figure 2 - High resolution STM image of a graphene monolayer on 3C SiC (111) obtained after annealing at 1250 ˚C. V_{bias}= 0.2V; I=80pA. The honeycomb structure is quite clear, the wrinkles are due to steps and defects in the underlying substrate.

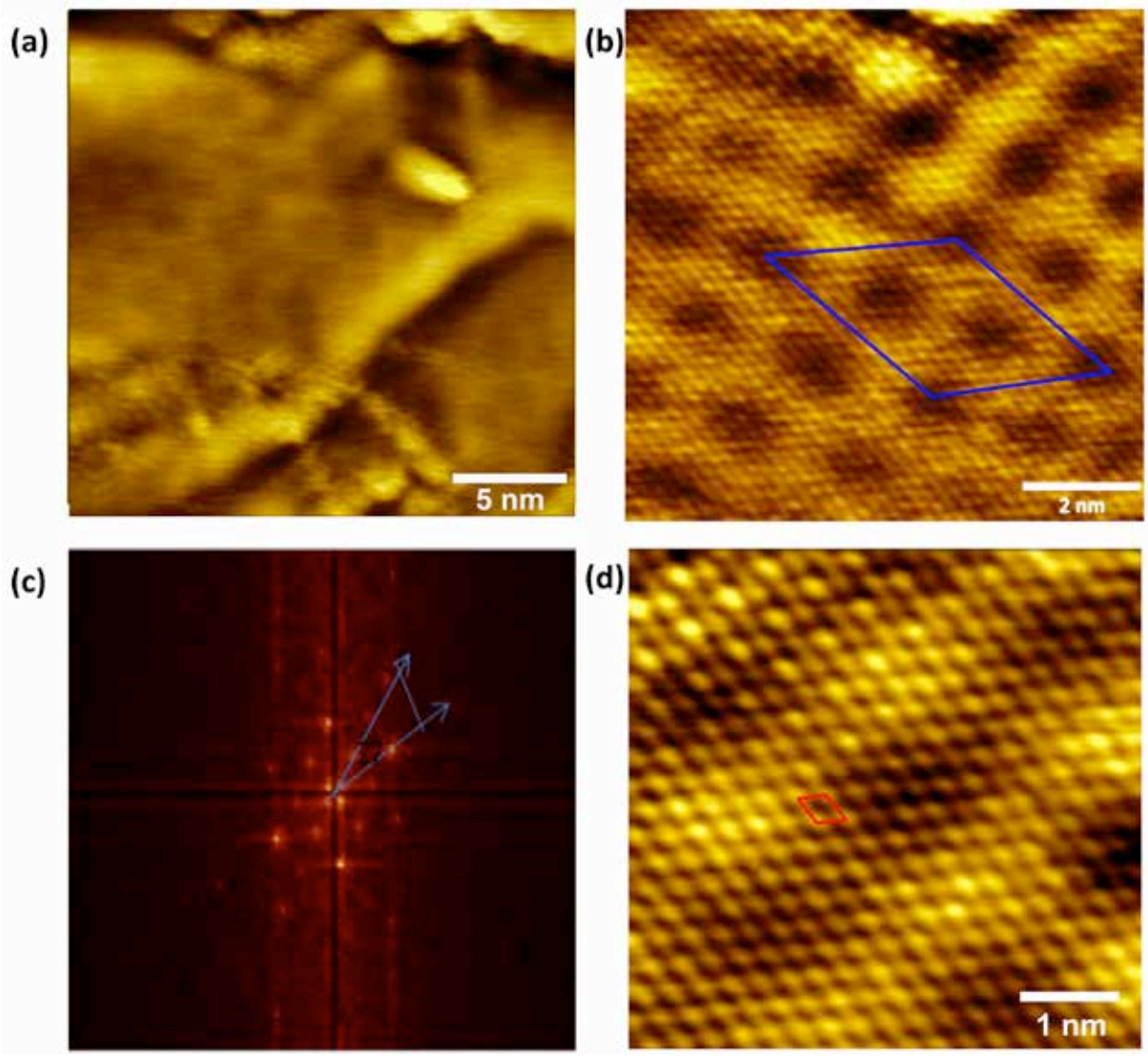

Figure 3 - STM images of graphene obtained by annealing SiC/Si(111) at 1300 ˚C. (a) 20x20 nm^2 area with a step showing a shadow of Moire pattern (V=70 mV, I=0.3 nA), (b) high resolution Moirè pattern with hexagonal symmetry (V=50 mV, I=0.2 nA). A ($6\sqrt{3}\times6\sqrt{3}$) R 30˚ unit cell (blue insert) is also shown, (c) FFT of image (b) showing 27˚ rotation of graphene layer with respect to the buffer layer and (d) high resolution STM image of bi/few layer graphene (V= 50 mV, I= 0.2 nA) with graphene unit cell (red insert).

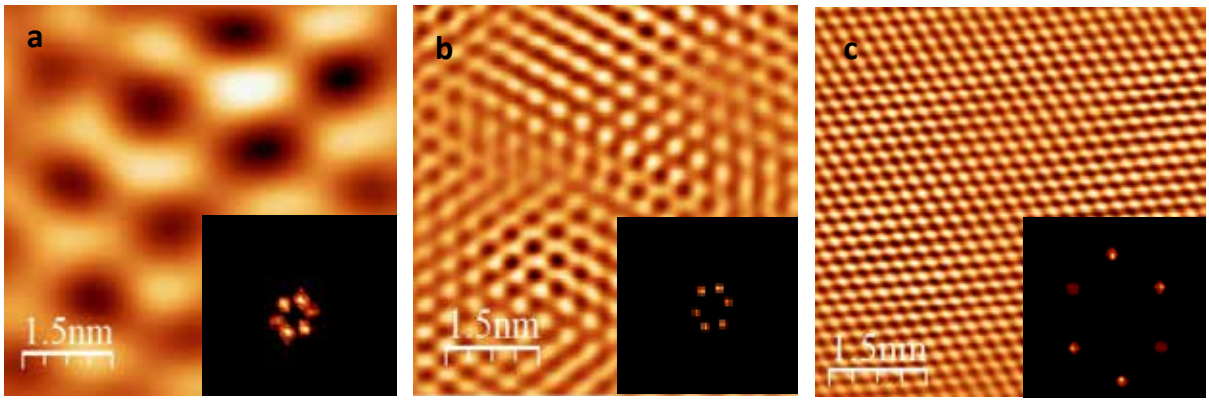

Figure 4 - FFT images extracted by selecting three hexagons of spots in Fig3c, as shown in the insets : (a) Moirè pattern from the innermost hexagon (b) second nearest neighbours from the middle hexagon and (c) first nearest neighbours (in the three-for-six symmetry of graphene atoms) from the outer hexagon.

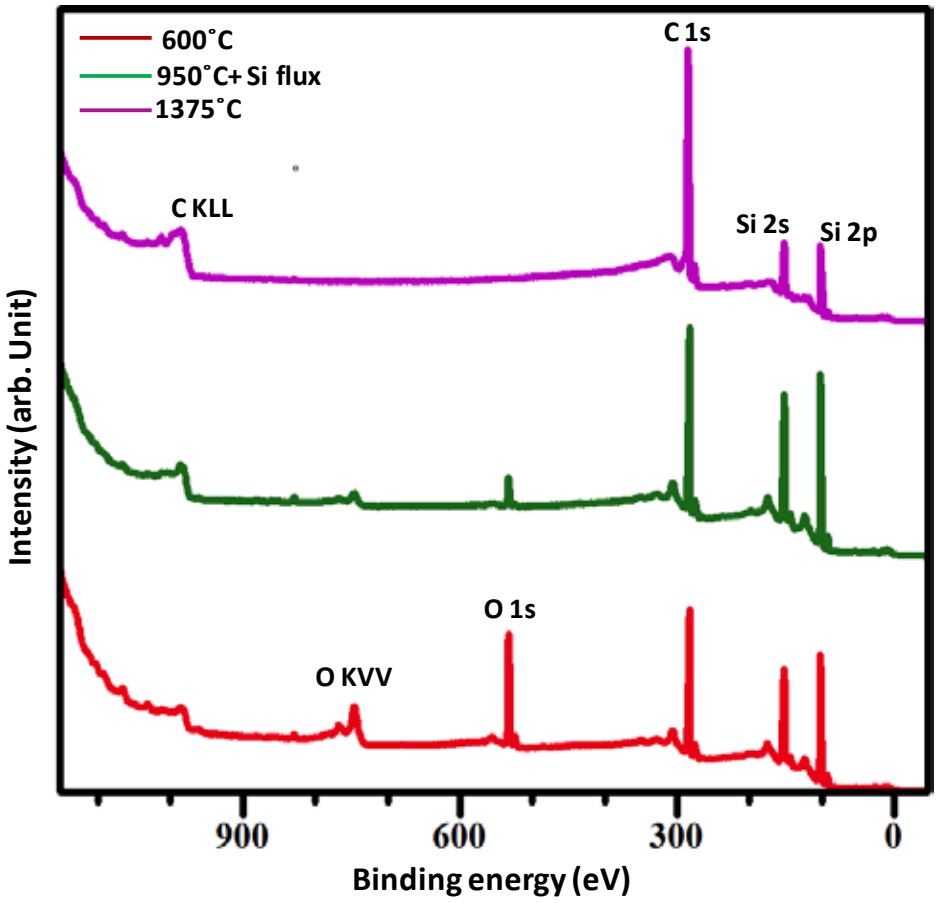

Figure 5 – Wide range XPS spectra of sample degassed at 600˚C, followed by Si flux at 950˚C and annealed at 1375˚C.

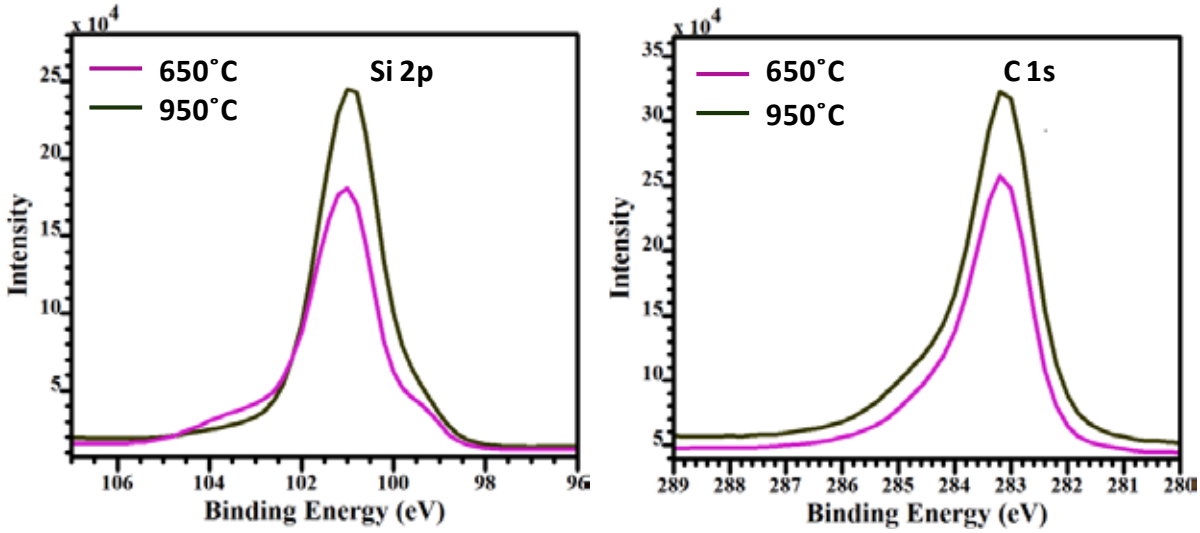

Figure 6 - X-ray Photoelectron Spectroscopy of the SiC (111) Si rich surface after 650 ˚C and 950˚C annealing with Si flux: (a) Si 2p and (b) C 1s

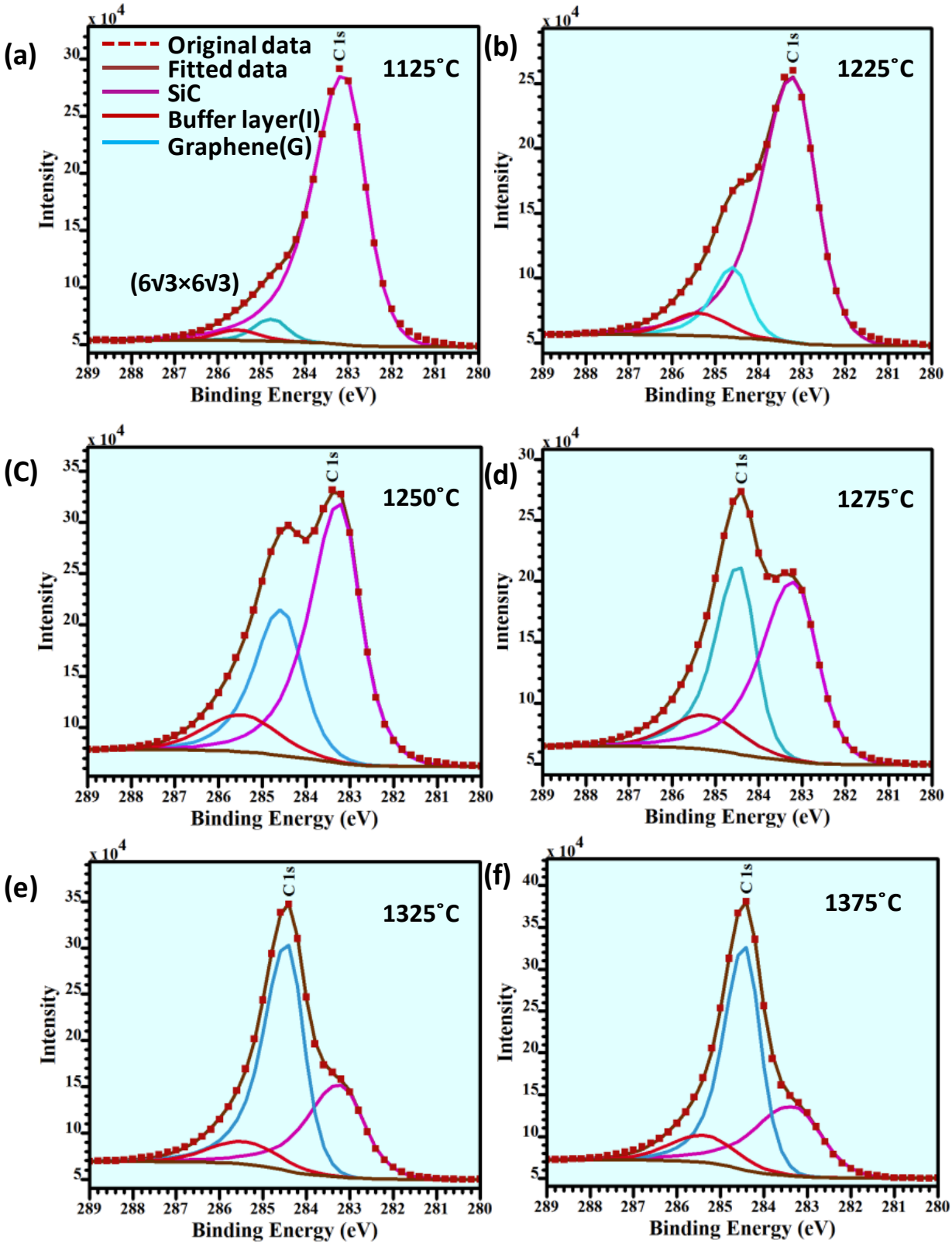

Figure 7 - C 1s XPS spectra for graphene growth as a function of increasing temperature. The sample was annealed at (a) 1125˚C (b) 1225˚C (c) 1250˚C (d) 1325˚C and (e) 1375˚C.

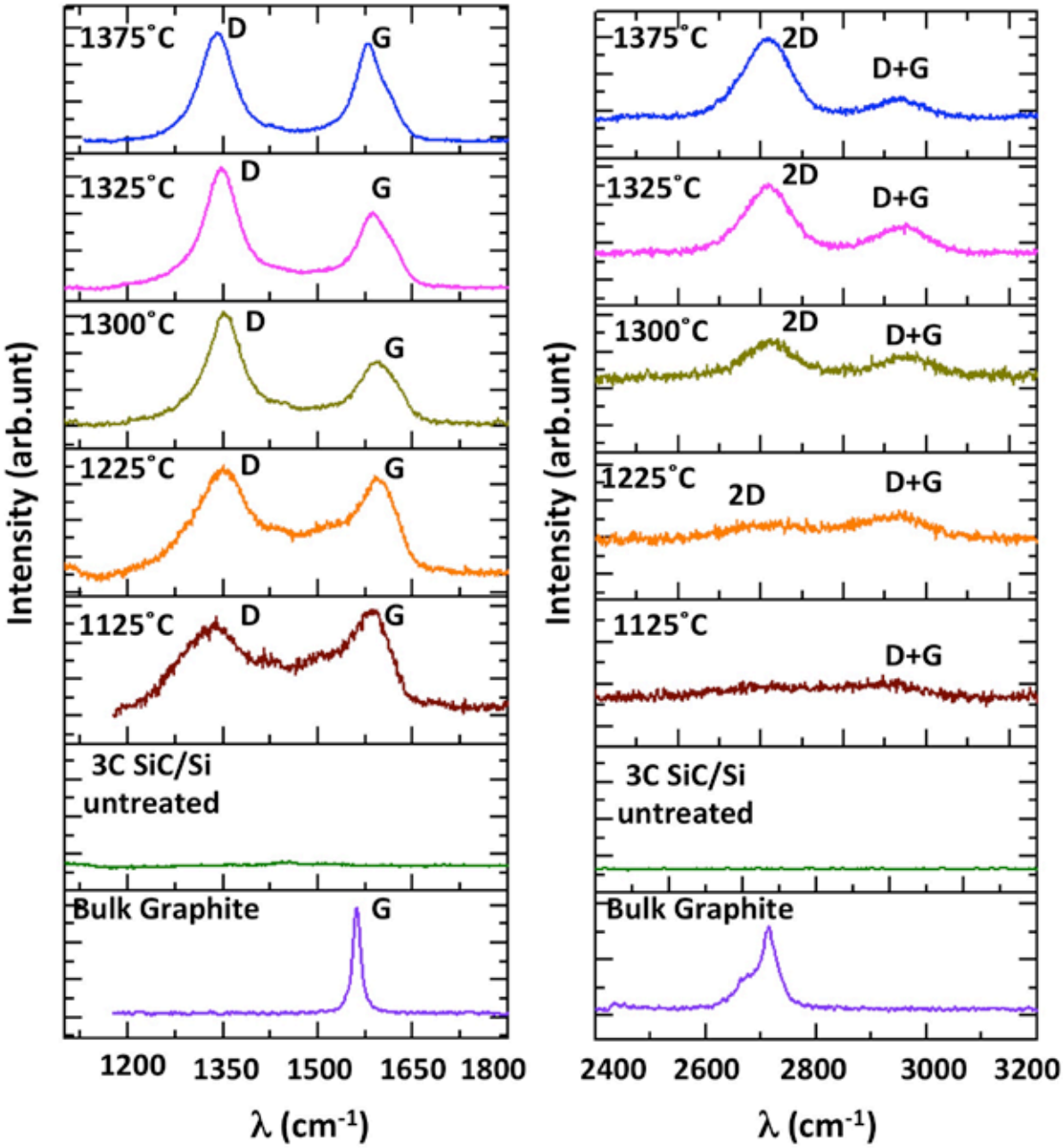

Figure 8 Raman spectra of bulk graphite, untreated 3C SiC/Si(111) substrate, samples annealed at 1125˚C, 1225˚C, 1300˚C, 1325˚C and 1375˚C (bottom- to-top). The Raman peaks are labelled following the standard identification.

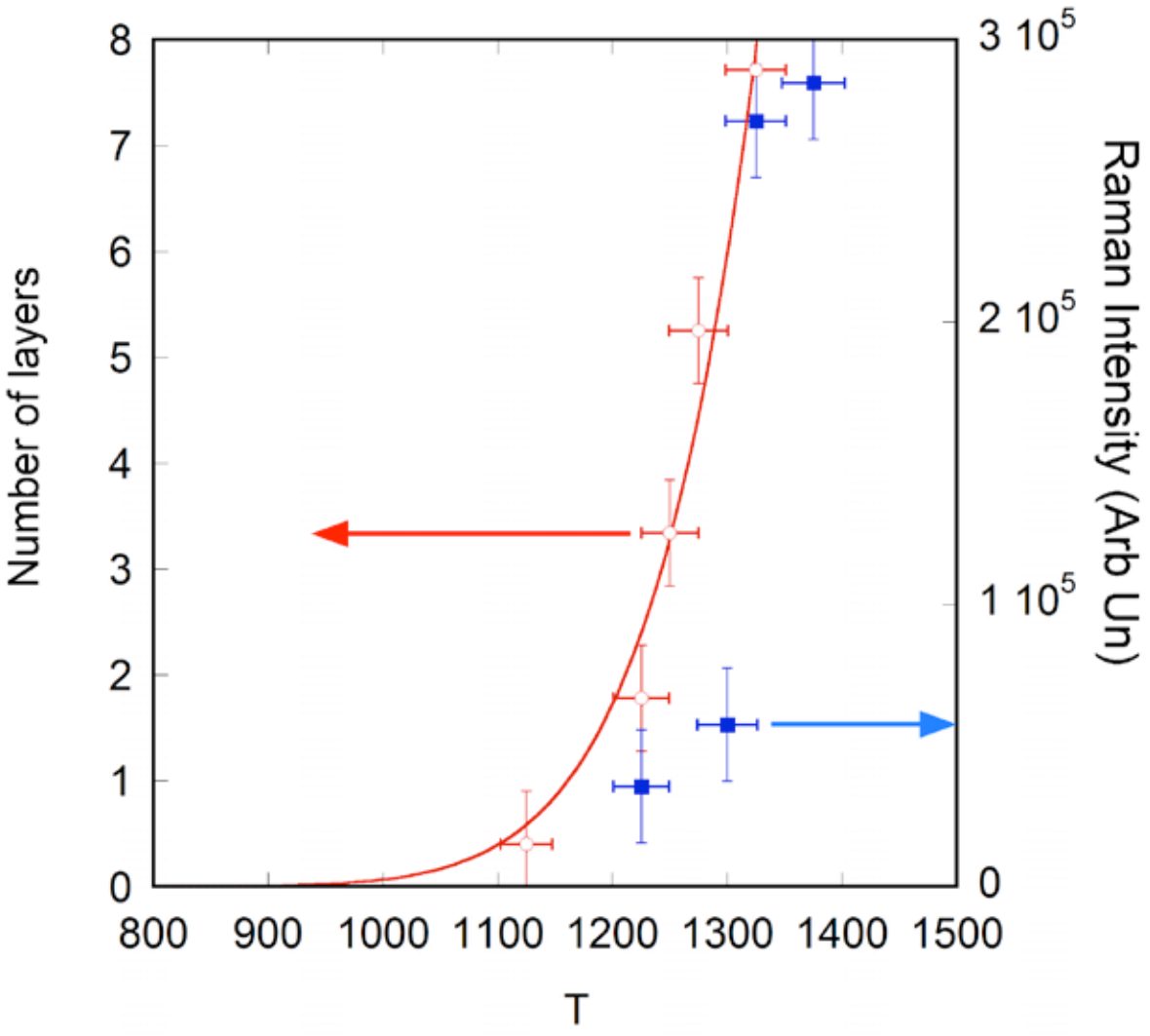

Figure 9 - Number of graphene layers developed in 10' versus annealing temperature, as obtained from XPS analysis (red circles). The values are fitted to an Arrhenius function (solid line). Blue squares: area of 2D Raman peak versus the annealing temperature.

TABLES

Table 1- FWHM and intensities of graphitic carbon and carbon peak of SiC calculated from peak fitting of XPS data. Average error in intensity values is ± 5%.

	Graphitic carbon (284.4)			Carbon peak of SiC (~283.2)		
Temperature	FWHM	Intensity (10^4 cps)	Atomic conc. (%)	FWHM	Intensity (10^4 cps)	Atomic conc. (%)
1125°C	0.81	1.9	4.5	1.12	40.5	93
1225°C	0.79	6.4	14	1.18	37.0	80
1250°C	1.07	21.7	31	1.07	41.6	59
1275°C	0.86	20.2	51	1.22	27.0	38
1325°C	0.86	3.21	58	1.25	18.0	33
1375°C	0.81	3.14	59	1.51	17.6	33

Table 2- Calculated number of graphene layers as a function of the annealing temperature

Annealing Temperature (°C)	1125	1225	1250	1275	1325	1375
Graphene layers	0.40±0.5	1.78±0.5	3.34±0.5	5.25±0.5	7.71±0.5	7.8±0.5

Table 3- G and 2D band positions, intensities and their FWHM

Temperature (˚C)	G-band			2D-band		
	position (cm^{-1})	Area	FWHM	position (cm^{-1})	Area	FWHM
Untreated 3C SiC/Si(111)	0	0	0	0	0	0
1125˚C	1612	99430	77. 49	0	0	0
1225˚C	1609	209352	70.31	2712	35380	115.3
1300˚C	1605	261031	67.83	2715	57373	104.69
1325˚C	1596	730128	63.16	2716	271027	101.77
1375˚C	1594	643843	57.40	2718	284584	96.46
Graphite	1580.46	23454	15.52	2720.06	40053	38.05

References

[1] K. Novoselov, A. K. Geim, S. Morozov, D. Jiang, Y. Zhang, S. Dubonos, I. Grigorieva, and A. Firsov, "Electric field effect in atomically thin carbon films," *Science,* vol. 306, pp. 666-669, 2004.

[2] R. Nair, P. Blake, A. Grigorenko, K. Novoselov, T. Booth, T. Stauber, N. Peres, and A. Geim, "Fine structure constant defines visual transparency of graphene," *Science,* vol. 320, pp. 1308-1308, 2008.

[3] A. A. Balandin, S. Ghosh, W. Bao, I. Calizo, D. Teweldebrhan, F. Miao, and C. N. Lau, "Superior thermal conductivity of single-layer graphene," *Nano letters,* vol. 8, pp. 902-907, 2008.

[4] C. Lee, X. Wei, J. W. Kysar, and J. Hone, "Measurement of the elastic properties and intrinsic strength of monolayer graphene," *Science,* vol. 321, pp. 385-388, 2008.

[5] K. S. Novoselov, Z. Jiang, Y. Zhang, S. Morozov, H. Stormer, U. Zeitler, J. Maan, G. Boebinger, P. Kim, and A. Geim, "Room-temperature quantum Hall effect in graphene," *Science,* vol. 315, pp. 1379-1379, 2007.

[6] M. Katsnelson, K. Novoselov, and A. Geim, "Chiral tunnelling and the Klein paradox in graphene," *Nature Physics,* vol. 2, pp. 620-625, 2006.

[7] A. Reina, X. Jia, J. Ho, D. Nezich, H. Son, V. Bulovic, M. S. Dresselhaus, and J. Kong, "Large area, few-layer graphene films on arbitrary substrates by chemical vapor deposition," *Nano letters,* vol. 9, pp. 30-35, 2008.

[8] M. Orlita, C. Faugeras, P. Plochocka, P. Neugebauer, G. Martinez, D. K. Maude, A.-L. Barra, M. Sprinkle, C. Berger, and W. A. de Heer, "Approaching the Dirac point in high-mobility multilayer epitaxial graphene," *Physical review letters,* vol. 101, p. 267601, 2008.

[9] A. K. Geim, "Graphene: status and prospects," *Science,* vol. 324, pp. 1530-1534, 2009.

[10] M. Shafiei, P. G. Spizzirri, R. Arsat, J. Yu, J. du Plessis, S. Dubin, R. B. Kaner, K. Kalantar-Zadeh, and W. Wlodarski, "Platinum/graphene nanosheet/SiC contacts and their application for hydrogen gas sensing," *The Journal of Physical Chemistry C,* vol. 114, pp. 13796-13801, 2010.

[11] M. Shafiei, K. Shin, J. Yu, S. Han, J. Jong, N. Motta, J. du Plessis, and W. Wlodarski, "Hydrogen gas sensing performance of a Pt/graphene/SiC device," 2011, pp. 170-173.

[12] K. S. Novoselov, "Nobel Lecture: Graphene: Materials in the Flatland," *Reviews of Modern Physics,* vol. 83, pp. 837-849, 2011.

[13] S. V. Morozov, K. S. Novoselov, M. I. Katsnelson, F. Schedin, D. C. Elias, J. A. Jaszczak, and A. K. Geim, "Giant Intrinsic Carrier Mobilities in Graphene and Its Bilayer," *Physical Review Letters,* vol. 100, p. 016602, 2008.

[14] K. I. Bolotin, K. J. Sikes, Z. Jiang, M. Klima, G. Fudenberg, J. Hone, P. Kim, and H. L. Stormer, "Ultrahigh electron mobility in suspended graphene," *Solid State Communications,* vol. 146, pp. 351-355, 2008.

[15] A. K. Geim and K. S. Novoselov, "The rise of graphene," *Nature materials,* vol. 6, pp. 183-191, 2007.

[16] L. G. De Arco, Y. Zhang, A. Kumar, and C. Zhou, "Synthesis, transfer, and devices of single-and few-layer graphene by chemical vapor deposition," *Nanotechnology, IEEE Transactions on,* vol. 8, pp. 135-138, 2009.

[17] S. Stankovich, D. A. Dikin, R. D. Piner, K. A. Kohlhaas, A. Kleinhammes, Y. Jia, Y. Wu, S. B. T. Nguyen, and R. S. Ruoff, "Synthesis of graphene-based nanosheets via

chemical reduction of exfoliated graphite oxide," *Carbon,* vol. 45, pp. 1558-1565, 2007.
[18] D. V. Kosynkin, A. L. Higginbotham, A. Sinitskii, J. R. Lomeda, A. Dimiev, B. K. Price, and J. M. Tour, "Longitudinal unzipping of carbon nanotubes to form graphene nanoribbons," *Nature,* vol. 458, pp. 872-876, 2009.
[19] H. Santos, L. Chico, and L. Brey, "Carbon nanoelectronics: unzipping tubes into graphene ribbons," *Physical review letters,* vol. 103, p. 86801, 2009.
[20] H. Kageshima, H. Hibino, and S. Tanabe, "The physics of epitaxial graphene on SiC (0001)," *Journal of Physics: Condensed Matter,* vol. 24, p. 314215, 2012.
[21] C. Riedl, C. Coletti, and U. Starke, "Structural and electronic properties of epitaxial graphene on SiC (0 0 0 1): a review of growth, characterization, transfer doping and hydrogen intercalation," *Journal of Physics D: Applied Physics,* vol. 43, p. 374009, 2010.
[22] J. L. Tedesco, B. L. VanMil, R. L. Myers-Ward, J. M. McCrate, S. A. Kitt, P. M. Campbell, G. G. Jernigan, J. C. Culbertson, C. Eddy Jr, and D. K. Gaskill, "Hall effect mobility of epitaxial graphene grown on silicon carbide," *Applied Physics Letters,* vol. 95, p. 122102, 2009.
[23] C. Berger, Z. Song, X. Li, X. Wu, N. Brown, C. Naud, D. Mayou, T. Li, J. Hass, and A. N. Marchenkov, "Electronic confinement and coherence in patterned epitaxial graphene," *Science,* vol. 312, pp. 1191-1196, 2006.
[24] I. Forbeaux, J. M. Themlin, A. Charrier, F. Thibaudau, and J. M. Debever, "Solid-state graphitization mechanisms of silicon carbide 6H-SiC polar faces," *Applied surface science,* vol. 162, pp. 406-412, 2000.
[25] A. Van Bommel, J. Crombeen, and A. Van Tooren, "LEED and Auger electron observations of the SiC (0001) surface," *Surface Science,* vol. 48, pp. 463-472, 1975.
[26] K. R. Ratinac, W. Yang, S. P. Ringer, and F. Braet, "Toward Ubiquitous Environmental Gas Sensors-Capitalizing on the Promise of Graphene," *Environmental Science & Technology,* vol. 44, pp. 1167-1176, Feb 15 2010.
[27] K. S. Novoselov, V. I. Falko, L. Colombo, P. R. Gellert, M. G. Schwab, and K. Kim, "A roadmap for graphene," *Nature,* vol. 490, pp. 192-200, 2012.
[28] A. Severino, C. Bongiorno, N. Piluso, M. Italia, M. Camarda, M. Mauceri, G. Condorelli, M. Di Stefano, B. Cafra, and A. La Magna, "High-quality 6inch (111) 3C-SiC films grown on off-axis (111) Si substrates," *Thin Solid Films,* vol. 518, pp. S165-S169, 2010.
[29] F. Iacopi, G. Walker, L. Wang, L. Malesys, S. Ma, B. V. Cunning, and A. Iacopi, "Orientation-dependent stress relaxation in hetero-epitaxial 3C-SiC films," *Applied Physics Letters,* vol. 102, pp. 011908-4, 2013.
[30] L. Wang, S. Dimitrijev, J. Han, A. Iacopi, L. Hold, P. Tanner, and H. B. Harrison, "Growth of 3C–SiC on 150-mm Si (100) substrates by alternating supply epitaxy at 1000° C," *Thin solid films,* vol. 519, pp. 6443-6446, 2011.
[31] A. Ouerghi, R. Belkhou, M. Marangolo, M. Silly, S. El Moussaoui, M. Eddrief, L. Largeau, M. Portail, and F. Sirotti, "Structural coherency of epitaxial graphene on 3C–SiC (111) epilayers on Si (111)," *Applied Physics Letters,* vol. 97, p. 161905, 2010.
[32] K. V. Emtsev, A. Bostwick, K. Horn, J. Jobst, G. L. Kellogg, L. Ley, J. L. McChesney, T. Ohta, S. A. Reshanov, and J. Röhrl, "Towards wafer-size graphene layers by atmospheric pressure graphitization of silicon carbide," *Nature materials,* vol. 8, pp. 203-207, 2009.
[33] P. Sutter, "Epitaxial graphene: How silicon leaves the scene," *Nat Mater,* vol. 8, pp. 171-172, 2009.

[34] A. Ouerghi, M. G. Silly, M. Marangolo, C. Mathieu, M. Eddrief, M. Picher, F. Sirotti, S. El Moussaoui, and R. Belkhou, "Large-Area and High-Quality Epitaxial Graphene on Off-Axis SiC Wafers," *Acs Nano,* vol. 6, pp. 6075-6082, 2012.
[35] R. Takahashi, H. Handa, S. Abe, K. Imaizumi, H. Fukidome, A. Yoshigoe, Y. Teraoka, and M. Suemitsu, "Low-Energy-Electron-Diffraction and X-ray-Phototelectron-Spectroscopy Studies of Graphitization of 3C-SiC (111) Thin Film on Si (111) Substrate," *Japanese Journal of Applied Physics,* vol. 50, p. 0103, 2011.
[36] U. Starke, C. Coletti, K. Emtsev, A. A. Zakharov, T. Ouisse, and D. Chaussende, "Large Area Quasi-Free Standing Monolayer Graphene on 3C-SiC (111)," 2012, pp. 617-620.
[37] L. Li and I. Tsong, "Atomic structures of 6H SiC (0001) and (000$\bar{1}$) surfaces," *Surface Science,* vol. 351, pp. 141-148, 1996.
[38] R. Kaplan and T. Parrill, "Reduction of SiC surface oxides by a Ga molecular beam: LEED and electron spectroscopy studies," *Surface Science,* vol. 165, pp. L45-L52, 1986.
[39] H. Huang, W. Chen, S. Chen, and A. T. S. Wee, "Bottom-up Growth of Epitaxial Graphene on 6H-SiC(0001)," *Acs Nano,* vol. 2, pp. 2513-2518, 2008/12/23 2008.
[40] A.Ouerghi, A. Kahouli, D. Lucot, M. Portail, L. Travers, J. Gierak, J. Penuelas, P. Jegou, A. Shukla, and T. Chassagne, "Epitaxial graphene on cubic SiC (111)/ Si (111) substrate," *Applied Physics Letters,* vol. 96, pp. 191910-3, 2010.
[41] S. L. Wong, H. Huang, W. Chen, and A. T. S. Wee, "STM studies of epitaxial graphene," *MRS Bulletin,* vol. 37, pp. 1195-1202, 2012.
[42] A. Ouerghi, A. Balan, C. Castelli, M. Picher, R. Belkhou, M. Eddrief, M. Silly, M. Marangolo, A. Shukla, and F. Sirotti, "Epitaxial graphene on single domain 3C-SiC (100) thin films grown on off-axis Si (100)," *Applied Physics Letters,* vol. 101, p. 21603, 2012.
[43] K. Emtsev, F. Speck, T. Seyller, L. Ley, and J. Riley, "Interaction, growth, and ordering of epitaxial graphene on SiC {0001} surfaces: A comparative photoelectron spectroscopy study," *Physical Review B,* vol. 77, p. 155303, 2008.
[44] M. Ridene, J. Girard, L. Travers, C. David, and A. Ouerghi, "STM/STS investigation of edge structure in epitaxial graphene," *Surface Science,* vol. 606, pp. 1289-1292, 2012.
[45] T. Seyller, "Structural and electronic properties of graphite layers grown on siC (0001)," *Surface Science,* vol. 600, pp. 3906-3911, 2006.
[46] E. Rollings, G. H. Gweon, S. Zhou, B. Mun, J. McChesney, B. Hussain, A. Fedorov, P. First, W. De Heer, and A. Lanzara, "Synthesis and characterization of atomically thin graphite films on a silicon carbide substrate," *Journal of Physics and Chemistry of Solids,* vol. 67, pp. 2172-2177, 2006.
[47] S. Tougaard, "QUASES-IMFP-TPP2M program, ,http:// www.quases.com."
[48] G. A. Somorjai, *Chemistry in Two Dimensions: Surfaces*. Ithaca: Cornell Univ Pr, 1981.
[49] L. Malard, M. Pimenta, G. Dresselhaus, and M. Dresselhaus, "Raman spectroscopy in graphene," *Physics Reports,* vol. 473, pp. 51-87, 2009.
[50] A. Ferrari, J. Meyer, V. Scardaci, C. Casiraghi, M. Lazzeri, F. Mauri, S. Piscanec, D. Jiang, K. Novoselov, and S. Roth, "Raman spectrum of graphene and graphene layers," *Physical review letters,* vol. 97, p. 187401, 2006.
[51] X. Li, Y. Zhu, W. Cai, M. Borysiak, B. Han, D. Chen, R. D. Piner, L. Colombo, and R. S. Ruoff, "Transfer of large-area graphene films for high-performance transparent conductive electrodes," *Nano letters,* vol. 9, pp. 4359-4363, 2009.

[52] Z. H. Ni, W. Chen, X. F. Fan, J. L. Kuo, T. Yu, A. T. S. Wee, and Z. X. Shen, "Raman spectroscopy of epitaxial graphene on a SiC substrate," *Physical Review B,* vol. 77, p. 115416, 2008.
[53] L. Cancado, K. Takai, T. Enoki, M. Endo, Y. Kim, H. Mizusaki, A. Jorio, L. Coelho, R. Magalhaes-Paniago, and M. Pimenta, "General equation for the determination of the crystallite size< equation> L< sub> a</sub></equation> of nanographite by Raman spectroscopy," *Applied Physics Letters,* vol. 88, pp. 163106-163106-3, 2006.
[54] A. C. Ferrari, J. C. Meyer, V. Scardaci, C. Casiraghi, M. Lazzeri, F. Mauri, S. Piscanec, D. Jiang, K. S. Novoselov, S. Roth, and A. K. Geim, "Raman Spectrum of Graphene and Graphene Layers," *Physical review letters,* vol. 97, p. 187401, 2006.
[55] Y. Kawashima and G. Katagiri, "Fundamentals, overtones, and combinations in the Raman spectrum of graphite," *Physical Review B,* vol. 52, p. 10053, 1995.